Available online at www.sciencedirect.com
ScienceDirect
Journal of Nuclear Materials 375 (2008) 397–409
journal of nuclear materials
www.elsevier.com/locate/jnucmat

# New modelling of the U–O–Zr phase diagram in the hyper-stoichiometric region and consequences for the fuel rod liquefaction in oxidising conditions

M. Barrachin [a,*], P.Y. Chevalier [b,1], B. Cheynet [b,1], E. Fischer [b,1]

[a] *Institut de Radioprotection et Sûreté Nucléaire (IRSN), DPAM, SEMIC, B.P. 3, F-13115 St. Paul Lez Durance, France*
[b] *THERMODATA-INPG-CNRS, 6 Rue du Tour de l'Eau, F-38400 St. Martin d'Hères, France*

Received 5 November 2007; accepted 6 February 2008

**Abstract**

Liquidus and solidus temperatures were recently re-measured in the $UO_{2+x}$ composition domain by [D. Manara, C. Ronchi, M. Sheindlin, M. Lewis, M. Brykin, J. Nucl. Mater. 342 (2005) 148]. The main difference with the Latta and Fryxell's data [R.E. Latta, R.E. Fryxell, J. Nucl. Mater. 35 (1970) 195] data is that the Manara's transition temperatures were accurately determined using a self-crucible technique while the former data were obtained in a W crucible and then suspected of crucible contamination. According to these recent data, a new thermodynamic modelling of U–O phase diagram is here presented and introduced in the European NUCLEA thermodynamic database for corium applications. An important consequence of this new optimisation for safety applications is that a liquid phase may appear in the O–$UO_2$–$ZrO_2$ composition domain of the U–O–Zr phase diagram at 2600 K at atmospheric pressure (this temperature decreasing with increase of pressure, about 2500 K at 2 atm.). These temperatures can be associated with the temperature at which the fuel assembly could loose its integrity in oxidising conditions and then with what was observed in some of the VERCORS tests where fuel collapse was detected in the temperature range of 2400–2600 K (and quite differently from reducing test conditions) or in the PHEBUS tests where indications of early fuel collapse at 2500–2600 K were identified.


## 1. Introduction

During an hypothetical severe accident in a pressurized water reactor (PWR), the interaction between Zircaloy (Zry) cladding and urania ($UO_2$) fuel is the main degradation process leading to the destruction of the core geometry. In such an accident, the reactor fuel may experience a variety of atmospheric conditions which will determine the nature of the interaction and the temperature of fuel liquefaction. These conditions are dynamic and, during the transient of an accident, the fuel could be exposed to temperatures ranging between 900 and 2800 K and from highly oxidizing to reducing environments.

In strongly reducing environment, due to the very low oxygen concentration in the gaseous fluid, the Zry cladding in contact with the $UO_2$ fuel may extract oxygen from it and dissolve it. This interaction was studied by Hofmann [1] in the temperature range 1273–1973 K and by Hayward [2–5], Olander [6–10] and Veshchunov [11] from 2273 to 2673 K. The $UO_2$/Zry interaction reaction starts at $T \sim 1273$ K when expansion of materials leads to a close contact between fuel and cladding. At $T \sim 2023$ K, the cladding melts and at 2173 K, it forms eutectics according to the $UO_2$–(α-Zr(O)) pseudo binary phase diagram [12]. Above this temperature, the fuel dissolution starts, resulting in the liquefaction of fuel rods at temperatures 1000 K below the standard melting temperature of $UO_2$ (3120 K).

* Corresponding author. Tel.: +33 4 42 19 94 14; fax: +33 4 42 19 91 66.
*E-mail addresses:* marc.barrachin@irsn.fr (M. Barrachin), contact@thermodata.eu (P.Y. Chevalier, B. Cheynet, E. Fischer).
[1] Tel.: +33 4 76 42 76 90; fax: +33 4 76 63 15 37.

0022-3115/$ - see front matter © 2008 Elsevier B.V. All rights reserved.
doi:10.1016/j.jnucmat.2008.02.003

Under more realistic conditions of severe accident, when steam is present, a part of cladding is molten (if the temperature exceeds the melting temperature of α-Zr(O)) and located between the zirconia ($ZrO_2$) cladding layer and fuel pellet, and dissolves simultaneously both solid materials [13]. In this situation, fuel dissolution is competitive with cladding oxidation and the prediction of the temperature of loss of fuel rod geometry becomes a difficult task.

The exposure of fuel to highly oxidizing environments should strongly reduce the fuel dissolution since it is expected that Zry cladding is quickly and fully oxidized before formation of molten metallic Zircaloy able to dissolve the pellet. In this situation, fuel-cladding interaction is then considered to start at relatively high temperatures (2800 K) according the $UO_2$–$ZrO_2$ phase diagram [14]. However, experimental observations in recent tests conducted under highly oxidizing atmosphere, e.g. in some of the small scale VERCORS experiments [15] using irradiated $UO_2$ (from 38 GWd/tU to 70 GWd/tU) and in the two first in-pile integral PHEBUS FP tests performed with trace irradiated fuel (FPT0 test [16]) and with irradiated fuel (FPT1 [17], 23 GWd/tU $UO_2$) evidenced that the fuel rod liquefaction temperature was well below 2800 K, around 2500–2600 K. For some of the VERCORS tests, Pontillon et al. [15] assumed a possible explanation of such a reduction of liquefaction temperature of $UO_2$–$ZrO_2$ mixtures in a potential effect of $UO_2$–$ZrO_2$–FP (Fission products) interactions. As the authors themselves mentioned in their article, this is contradictory with the known unsignificant effect of burn-up on the melting temperature of urania as considered in [18] and measured in [19,20], at least up to a burn-up of 50 GWd/tU. For the PHEBUS tests, the interaction with the control rod materials present in the test bundle was assumed to explain at least partially the early degradation of fuel rods [16].

The exposure of fuel to oxidizing environments increases its oxygen potential after the Zry cladding is totally oxidized. As a result, the fuel stoichiometry increases, changing its material properties and in particular its melting temperature [21,22]. Up to very recently, the impact of fuel oxidation on its degradation was not considered as significant on the basis of the Latta and Fryxell's experimental data [21]. Considering the new measurements recently performed by Manara et al. [22] on the melting behavior of hyper-stoichiometric fuel, significantly different from the previously existing available information [21], the potential role of fuel oxidation on the fuel rod liquefaction process in oxidizing conditions should be re-considered.

In this paper, the first part (Part 2) is devoted to the new thermodynamic modeling of the U–O and U–O–Zr phase diagrams in the hyper-stoichiometric region. Indeed, the new liquidus and solidus data obtained in the $OU_{2+x}$ region make necessary to re-assess these phase diagrams previously presented [23]. In Part 3, are presented the post-mortem examinations of the PHEBUS FPT1 test and some of the VERCORS tests related to the fuel rod liquefaction. The interpretation of these examinations allows to evaluate the extent of the fuel-cladding interaction in oxidizing conditions and the impact of the fuel oxidation on the liquefaction process on the basis of the new modeling of the U–O–Zr phase diagram.

## 2. O–U and O–U–Zr phase diagrams revisited in the hyper-stoichiometric field

### 2.1. Introduction

In hyper-stoichiometric region (O/U > 2), the phase diagram of the binary system O–U [23] presents the following condensed phases:

- the liquid phase (L),
- the $UO_{2+x}$ solid solution, with the face-centered cubic structure (fcc_C1),
- three other intermediate oxides, $U_4O_{9-y}$, $U_3O_{8-z}$ and $UO_3$,
- the gas phase (G).

Up to now, the only existing experimental data at high temperature (> 2500 K) were solidus and liquidus temperatures over the composition range $UO_2$–$UO_{2.23}$ measured by Latta and Fryxell [21]. These results were suspected of crucible contamination by the authors themselves. The uncertainty on the real liquidus shape in the hyper-stoichiometric field led to obtain various temperatures in the literature for the invariant reaction $L <=> G + UO_{2+x}$ for 1 atm. total pressure: 3077 K (Chevalier et al. [23]); 2700 K (Gueneau et al. [24]), 2873 K (Roth et al. [25]). That's why the melting of stoichiometric and hyper-stoichiometric uranium dioxide was recently thoroughly investigated by means of advanced techniques by Manara et al. [22]. These new results allow to re-visit the modeling of the O–U phase diagram in the hyper-stoichiometric field previously published in [23] and to evaluate the impact of this new assessment on the calculation of the isothermal sections in the O–U–Zr ternary system at high temperature.

### 2.2. Experimental information for solidus/liquidus in $UO_{2+x}$ region

#### 2.2.1. Latta and Fryxell

Solidus and liquidus temperatures for $UO_{2\pm x}$ were firstly determined by Latta and Fryxell [21] by a thermal arrest technique, using samples sealed in tungsten (W) or rhenium (Re). The melting point of standard $UO_2$ was given as 3138 K. The absolute accuracy of the temperature measurements (±15 K) was checked by melting Ta, Mo and $Al_2O_3$ (sapphire) as standards. For $UO_{2\pm x}$, solidus and liquidus temperatures, respectively decreased down to 2837 K and 3031 K for O/U = 2.23 ($x$(U) = 0.3096) in the hyper-stoichiometric range. Experimental values are reported in Table 1. Eleven values are given for the liquidus (3013–3138 K) and solidus (2837–3120 K) for 2 < O/U < 2.23 (0.3096 < $x$(U) < 0.3333). Post-test microanalyses

Table 1
Experimental liquidus ($L/L + UO_{2+x}$) and solidus ($UO_{2+x}/UO_{2+x} + L$) in the hyper-stoichiometric range from Latta and Fryxell [21]

| O/U | $x$ (U) | $T^L$ (K) | $T^S$ (K) |
|---|---|---|---|
| 1.997 | 0.3337 | 3135 | 3120 |
| 1.998 | 0.3336 | 3138 | 3118 |
| 2.019 | 0.3312 | 3125 | 3109 |
| 2.022 | 0.3309 | 3136 | 3085 |
| 2.058 | 0.3270 | 3109 | 3067 |
| 2.095 | 0.3231 | 3090 | 3001 |
| 2.095 | 0.3231 | 3088 | 3003 |
| 2.120 | 0.3205 | 3071 | 2907 |
| 2.130 | 0.3195 | 3078 | 2940 |
| 2.184 | 0.3141 | 3045 | 2878 |
| 2.230 | 0.3096 | 3013 | 2851 |
| 2.230 | 0.3096 | 3031 | 2837 |

showed that, for O/U > 2.058, samples had interacted with the rhenium or tungsten capsules with significant losses of oxygen.

### 2.2.2. Manara et al. [22]

The recent work of Manara et al. [22] was performed in order to re-investigate experimentally the liquidus and solidus of the O–U system in the hyper-stoichiometric domain, $UO_{2+x}$. The reason of these new measurements was the suspected contamination of samples by crucible in the previous work of Latta and Fryxell [21]. These new data was obtained under containerless conditions and under buffer gas pressures up to 250 MPa, at which evaporation was ineffective, so that essential limits encountered in previous experiments could be overcome. Heating of the sample was performed by using laser that enables fast (ten of ms) melting/freezing processes. Thermograms were recorded with fast pyrometers, and the thermal arrest features were interpreted with the help of computer simulations. The determinations of the solidus and liquidus temperatures are corroborated by the detection of sample surface reflectivity variations (RLS method). During heat-up, the solidus temperature is assumed to be linked with the sudden reflectivity change due to appearance of liquid on the sample surface. During cooling down from temperatures above the liquidus, vibrations of the liquid cause oscillations of the reflected light intensity that disappear when the solidus is reached. The solidus is also determined from the visual examination of the surface. The melting line of $UO_{2.00}$ was for the first time determined in the pressure range between 0.1 and 250 Mpa. For the hyper-stoichiometric oxide, the liquidus and solidus lines, measured at pressures between 50 and 250 Mpa, significantly differ from the previous data. Experimental values are reported in Table 2.

### 2.2.3. Discussion

The comparison between Tables 1 and 2 show that there are large discrepancies between the different sets of experimental data. Solidus and liquidus measured by Latta and Fryxell [21] are generally higher than the values obtained by Manara et al. [22]. This is likely due to an uncontrolled of the sample composition in [21] and the interaction with the W or Re capsules which lowers the effective oxygen concentration in the tested samples.

Table 2
Experimental liquidus ($L/L + UO_{2+x}$) and solidus ($UO_{2+x}/UO_{2+x} + L$) in the hyper-stoichiometric range and associated uncertainties from Manara et al. [22]

| O/U | $x$ (U) | $T^L$ (K) | $dT^L$ | $dx^L$ | $T^S$ (K) | $dT^S$ | $dx^S$ |
|---|---|---|---|---|---|---|---|
| 2.00 | 0.3337 | 3147 | 20 | 0.005 | 3147 | 20 | 0.005 |
| 2.01 | 0.3336 | 3135 | 20 | 0.005 | 3071 | 20 | 0.005 |
| 2.03 | 0.3312 | 3130 | 20 | 0.005 | 3055 | 25 | 0.005 |
| 2.03 | 0.3312 | 3115 | 25 | 0.005 | 3060 | 25 | 0.005 |
| 2.05 | 0.3270 | 3098 | 20 | 0.005 | 2964 | 50 | 0.005 |
| 2.07 | 0.3231 | 3028 | 40 | 0.005 | 2948 | 40 | 0.005 |
| 2.07 | 0.3336 | 3070 | 20 | 0.005 | 2958 | 40 | 0.005 |
| 2.07 | 0.3312 | 3063 | 40 | 0.005 | 2954 | 40 | 0.005 |
| 2.08 | 0.3337 | 3075 | 20 | 0.010 | 2886 | 25 | 0.010 |
| 2.09 | 0.3336 | 3056 | 25 | 0.005 | 2901 | 49 | 0.005 |
| 2.11 | 0.3312 | 2995 | 20 | 0.015 | 2793 | 40 | 0.005 |
| 2.12 | 0.3309 | 3008 | 20 | 0.020 | 2699 | 25 | 0.010 |
| 2.12 | 0.3270 | 3020 | 25 | 0.020 | 2696 | 25 | 0.010 |
| 2.14 | 0.3231 | 2930 | 40 | 0.030 | 2607 | 25 | 0.010 |
| 2.16 | 0.3336 | 2920 | 30 | 0.035 | 2606 | 30 | 0.010 |
| 2.17 | 0.3312 | 2887 | 50 | 0.040 | 2528 | 50 | 0.005 |
| 2.17 | 0.3309 | 2891 | 25 | 0.040 | 2550 | 50 | 0.005 |
| 2.17 | 0.3337 | | | | 2530 | 50 | 0.005 |
| 2.20 | 0.3336 | 2865 | 30 | 0.055 | 2438 | 35 | 0.005 |
| 2.21 | 0.3312 | 2795 | 60 | 0.059 | 2410 | 25 | 0.005 |

For only one composition (O/U = 2.022), Latta and Fryxell [21] measured very few pollution in the sample after the test. The solidus and liquidus temperatures were determined at 3085 and 3136 K, respectively, i.e. in agreement with the measurements performed by Manara et al. [22] in the O/U range between 2.01 and 2.03 (Table 2).

To our opinion, different convincing arguments detailed in [22,26] are clearly in favor of the laser flash technique by comparison with the facility used by Latta and Fryxell [21]. They are the control of the composition of the sample during heating since there is no evaporation of oxygen due to the high imposed isostatic pressure, the absence of the crucible suppressing a possible interaction between the latter and the sample and finally the determination of the solidus and liquidus temperatures by different independent means. Nevertheless, the recent reviews of Baichi et al. [27,28] on U–O thermodynamics which discarded the Manara's experimental data show that there is no consensus about the reliability of the flash laser technique for the determination of the solidus/liquidus temperatures in the hyper-stoichiometric region of the U–O phase diagram.

For the liquidus determination in [22], both thermal arrest detection and RLS method are applied during the cooling stage. One of the main arguments developed in [27,28] against the employed methodology is the possible formation of metastable phases due to the large quenching speed (about 10000 K/s) in the laser flash technique. In applying a too high cooling rate, undercooling may happen. In these non equilibrium conditions, solid phase

may not appear below the liquidus temperature. At a certain temperature, formation of solid phase takes place and the released fusion enthalpy heats up the sample until the liquidus temperature is reached, provoking an inflexion on the thermal curve. The completion of this recovery is mainly dependent on the cooling rate, the nature of the material and the mass of the melted sample which participates to the process. In particular, if this mass is not significant, the energy released by the phase change may be too small to achieve a complete recovery. The measurement of the melting temperature of stoichiometric $UO_2$ in [22] with a similar quenching rate that for $UO_{2+x}$ shows that this recovery is small (few kelvins) but complete if we consider the agreement between the measurement and the usual recommended value for the melting temperature of $UO_2$. It pleads for the suitability of the quenching conditions used in [22].

For the solidus determination in [22], the RLS method and the visual inspection of the sample are considered during the heating stage. It cannot be excluded that, in case of samples very inhomogeneous, liquid is firstly formed only at sites far from the surface and then neither RLS nor the visual examination of the sample are adequate techniques to determine the solidus temperature. For $UO_{2+x}$, considering the preparation of the samples in [22], this difficulty should be overcome.

A review of bibliography shows that the laser flash method was employed to measure solidus and liquidus temperatures in different studies and in particular for U–O–Zr compositions. These compositions are of interest for the validation of the experimental methodology because, as $UO_{2+x}$, they correspond to non congruently liquefactions and for some of them, comparisons can be performed with data obtained in different experimental conditions. Two studies are of particular interest:

– Ronchi and Sheindlin [29] determined melting temperatures for different $(U,Zr)O_2$ oxide compositions from the thermal arrest on thermograms during cooling. The so-called melting temperature seems to correspond to the solidus temperature as mentioned in [29] since it is determined from the second thermal arrest on the cooling curve. The obtained values can be compared to the data of Lambertson et al. [14] in which samples of different $(U,Zr)O_2$ compositions were heated, maintained at desired temperature, quenched and finally examined by X-diffraction. A good agreement (Table 3) is observed between both experimental sets of data.

Table 3
Solidus temperatures determined by Ronchi et al. [29] for $(U,Zr)O_2$ compositions and comparison with experimental data of Lambertson et al. [14]

| Composition | [29] | Composition | [14] |
|---|---|---|---|
| $(U_{0.5}Zr_{0.5})O_2$ | $2805 \pm 5$ | $(U_{0.486}Zr_{0.514})O_2$ | $2790 \pm 25$ |
| $(U_{0.2}Zr_{0.8})O_2$ | $2810 \pm 5$ | $(U_{0.228}Zr_{0.772})O_2$ | $2771 \pm 25$ |
| | | $(U_{0.162}Zr_{0.838})O_2$ | $2826 \pm 25$ |

– By using the same procedure that in [22], Bottomley et al. [30] recently measured solidus and liquidus of different hypostoichiometric U–O–Zr compositions on the composition line $UO_2$–Zr. For one of these compositions (U–Zr–O = 22–33–45 at.%), the liquidus and solidus temperatures were also determined for benchmark within the ISTC CORPHAD Project [31] by the technique of the visual polythermal analysis (VPA) described in [32]. An agreement is obtained between the two experimental data for the liquidus as well as for the solidus. The liquidus temperature was measured in agreement with the modeling of the U–O–Zr phase diagram as presented in [23]. By contrast, the solidus temperature values, in both studies, were found at an unexpected high temperature (about 2600 K) considering the experimental results of Hofmann and Kerwin-Peck [1] which put in evidence, at temperatures as low as 1423 K, the formation of a liquid phase resulting of a solid state interaction between $UO_2$ and Zry. The erroneous detections of the solidus temperature in [30,31] could be due to the heterogeneous nature of the interfacial reaction between $UO_2$ and Zry [33] which make difficult the visual detection of solidus by RLS or VPA.

These different studies tend to prove the reliability of the laser flash technique and the methods of determination for the liquidus used in [22]. For the solidus measurements, problems of detections may occur in case of inhomogeneous samples. For $UO_{2+x}$, such problems should not be encountered.

### 2.3. Thermodynamic modeling

#### 2.3.1. Introduction

In a general way, the Gibbs energy ($G$) of a condensed solution phase is the sum of several terms (reference, ideal, excess):

$$G = G^{\mathrm{ref}} + G^{\mathrm{id}} + G^{\mathrm{ex}}. \quad (1)$$

Within this formalism, the different condensed phases in the hyper-stoichiometric region of the O–U phase diagram have to be considered:

– The small non-stoichiometry range of the two compounds $U_4O_{9-y}$ and $U_3O_{8-z}$ are not modelled. $U_4O_{9-y}$ and $UO_3$ both decompose below 1500 K and thus do not apply for the present studied severe accident conditions. They are all considered as stoichiometric. The Gibbs energies of these compounds are given in [23].
– The liquid phase, ($L$), is represented by means of the associate model, basically described by Dolezalek [34] and by Prigogine and Defay [35]. It is assumed to be a non ideal mixture of pure species, oxygen, $O_1(L)$, and uranium, $U_1(L)$, and associated species, uranium dioxide, $O_2U_1(L)$. The expressions of the different terms of (1) are detailed in [23]. In particular, the excess Gibbs energy of the liquid phase is defined as

$$G^{ex}(L) = y(O_1)y(U_1)L[O_1,U_1]\langle L\rangle + y(O_1)y(O_2U_1)L[O_1,O_2U_1]\langle L\rangle + y(O_2U_1)y(U_1)L[O_2U_1,U_1]\langle L\rangle.$$

where $y(i)$ is the concentration in $i$ and $L[i,k]<L>$, the interaction parameter between $i$ and $k$ species in the liquid, $L$. The interaction parameter, $L[i,k]<L>$ is described by using a Redlich–Kister type polynomial expression

$$L[i,k]\langle L\rangle = \Sigma_v L^{(v)}[i,k]\langle L\rangle(y(i)-y(k))^v.$$

The $L^{(v)}[i,k]<L>$ parameters may vary with temperature.

As the $O_1$ species are predominant in the hyper-stoichiometric domain, the excess Gibbs energy of the liquid phase in this concentration region is mainly described by the mean of the interaction parameter between $O_1$ and $O_2U_1$, $L[O_1, O_2\ U_1]<L>$, this parameter being optimized by using the solidus and liquidus experimental data for $UO_{2+x}$, in conjunction with the modeling of the $UO_{2+x}$ solid solution.

– The $UO_{2+x}$ solid solution is modeled by a multi sublattice model, initially introduced by Sundman and Agren [36]. Its Gibbs energy is represented with a three sublattice model with defects (vacancies Va, and interstitials) which allows to describe the hyper-stochiometric field. The choice of this model is discussed in detail in [37]. The formula for this model is summarized by the expression $(U)_1{}^{(1)}(O, Va)_2{}^{(2)}(O, Va)_1{}^{(3)}$. In the first lattice (1) are positioned the uranium atoms. The second lattice (2) is formed by the regular sites for oxygen atoms in the $UO_2$ fluorite structure with a stoichiometry of 2. These sites can be partially vacant. In the third lattice (3), oxygen interstitials are included in order to be able to describe the thermodynamics of the hyper-stoichiometric region. For this three sub-lattice model, the expressions of the different terms of relation (1) are detailed by Chevalier et al. [23]. In particular, the excess Gibbs energy is defined as

$$G^{ex}(L) = y^{(3)}(O_1)y^{(2)}(O_1)y^{(2)}(Va)L[U_1][O_1,Va]_2[O_1]\langle fcc\_C1\rangle + y^{(3)}(Va)y^{(2)}(O_1)y^{(2)}(Va)L[U_1][O_1,Va]_2[Va]\langle fcc\_C1\rangle + y^{(2)}(O_1)y^{(3)}(O_1)y^{(3)}(Va)L[U_1][O_1]_2[O_1,Va]\langle fcc\_C1\rangle + y^{(2)}(Va)y^{(3)}(O_1)y^{(3)}(Va)L[U_1][Va]_2[O_1,Va]\langle fcc\_C1\rangle$$

where $y^{(p)}(i)$ is the concentration in $i$ on sublattice $p$ and $L[j][i,k][l]<fcc\_C1>$, the interaction parameter between $i$ and $k$ species on the second sublattice, the first and the third sublattices being supposed completely fulfilled by the components $j$ and $l$, respectively. The interaction parameter, $L[j][i,k][l]<fcc\_C1>$ is described by using a Redlich–Kister type polynomial expression

$$L[j][i,k][l]\langle fcc\_C1\rangle = \Sigma_v L^{(v)}[j][i,k][l]\langle fcc\_C1\rangle(y(i)-y(k))^v$$

The $L^{(v)}[j][i,k][l]<fcc\_C1>$ parameters may vary with temperature.

Chevalier et al. [23] proved the capability of this model to represent the whole set of oxygen potential data in the temperature range 973–1773 K by showing the perfect agreement obtained from the graphical comparison at constant temperature of calculated values $RTln\ P(O_2) = f(O/U)$ (where $P(O_2)$ is the partial pressure of $O_2(G)$) with the experimental ones. Moreover, the limits and the oxygen potentials of the two di-phasic domains $UO_{2+x} + U_4O_9$ and $UO_{2+x} + U_3O_8$ are also very well reproduced, which also prove the self-consistency of the thermodynamic data of the solid solution and the two stoichiometric compounds below 2000 K.

At temperatures above 2000 K, a complex gaseous phase is present, modeled from the gaseous species (O, $O_2$, $O_3$, $O_3U$, $O_2U$, OU, U). The liquid phase, L, may appear at very high temperature ($T > 2500$ K): $L <=> G + UO_{2+x}$. The temperature of this invariant reaction is linked to the Gibbs energy of the liquid phase on the hyper-stoichiometric liquidus and varies with the total pressure. As the Gibbs energy in the $UO_{2+x}$ hyper-stoichiometric solid solution depends only on the extrapolation of the validated thermodynamic modeling at very high temperature (1800–3120 K), and was fixed by the conclusions of the work published in [23], the Gibbs energy of the liquid phase on the liquidus is well determined if the liquidus shape is also precisely known in this field. This is why the new results of [22] are of the prime importance for the modeling of the O–U system at high temperature.

### 2.3.2. New thermodynamic modelling of the O–U system

The Gibbs energies of the different phases of the O–U binary system have been optimized in the hyper-stoichiometric field, by taking into account new selected liquidus and solidus experimental data, recently determined by Manara et al. [22]. If one compares the assessed excess Gibbs energy parameters of the solution phases (liquid and solid) to ones published by Chevalier et al. [23] (Table 4), one can observe that the excess Gibbs energy parameters of the $UO_{2+x}$ solid solution are only slightly modified. It is quite normal, because they are optimized by taking into account the whole oxygen potential experimental database, $\{P(O_2) = f(x)\}$. However, no experimental data above 1800 K are available, and the extrapolated oxygen potential could be slightly different due to the difference of modeling of the liquidus/solidus experimental data. Thus, the slight modifications only come from the modification of constraints at higher temperatures, imposed by the new liquidus and solidus experimental data of Manara et al. [22]. Only the excess Gibbs energy parameters of the liquid phase are strongly modified.

In Fig. 2, the O–U phase diagram is calculated with a high pressure applied on it so that no vaporization can happen, as in the experimental conditions of [22]. The temperature of the peritectic reaction $L + UO_{2+x} <=> O_3U_8(S)$ in these conditions is calculated as 2411 K

Table 4
Excess Gibbs energy parameters of the condensed solution phases, liquid and $UO_{2+x}$(fcc_C1) in the hyper-stoichiometric domain $UO_{2+x}$

| Phase | Parameter | Values | |
|---|---|---|---|
| | | Chevalier et al. [23] | This work |
| Liquid | $L[O_1, O_2U_1]$ <L> | −71931.90 | −120620.04 |
| $UO_{2+x}$ | $L^0[U_1][O_1]_2[O_1, Va]$<fcc_C1> | −237337.50−51.79685T | −233515.51−51.93057T |
| | $L^1[U_1][O_1]_2[O_1, Va]$<fcc_C1> | −110992.28 | −109179.12 |
| | $G(O_3U(fcc\_C1))-1.5G(O_2(G))- G(U(ort\_A20))$ | −1089204.89 + 269.06381T | −1091293.17 + 269.09499T |

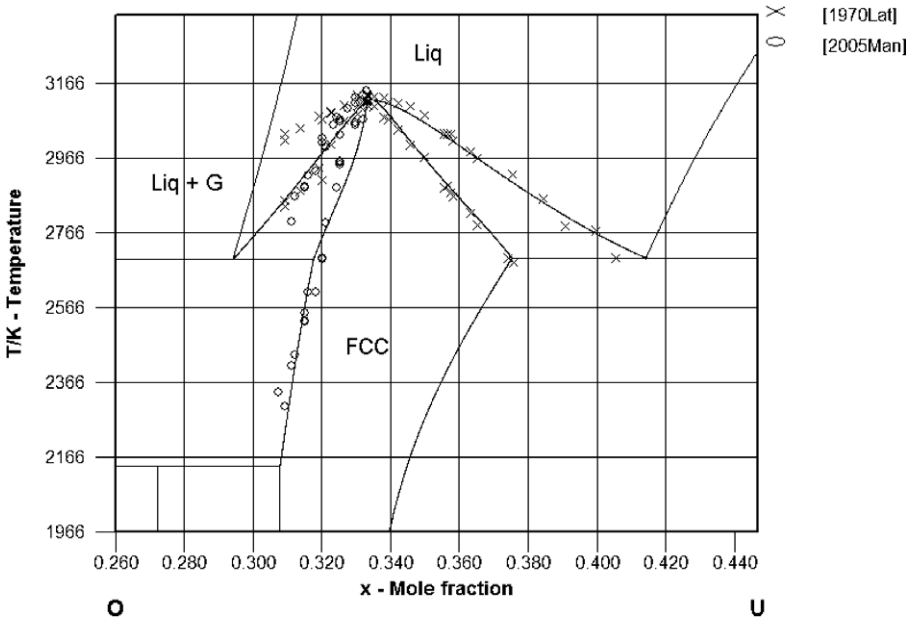


Fig. 1. Calculated phase diagram (fixed condition of $P_{tot} = 1$ atm) of the O–U binary system with new optimized parameters in the hyper-stoichiometric field $UO_{2+x}$ with superimposed experimental data from [21,22] (the gas phase is mentioned in the phase diagram only when the vapor pressure of the complex gaseous mixture of $O–O_2–O_3–O_3U–O_2U–OU–U$ reaches the total pressure, i.e. 1 atm, otherwise it means that the vapor pressure is lower than one atmosphere).

(Fig. 2). The solidus and the liquidus curves fit the experimental data produced by Manara et al. [22].

With a more reduced applied pressure, a complex gas phase $O–O_2–O_3–O_3U–O_2U–OU–U$ may appear. The vapour pressure and the composition of the gas phase varies along the liquidus and the solidus curves. The lowest temperature for which the vapor pressure in equilibrium reaches one atmosphere corresponds to the monotectic reaction $L <=> G + UO_{2+x}$ and is calculated as 2694 K (Fig. 1), instead of 3077 K previously [23]. For a vapour pressure in equilibrium of two atmospheres, the temperature of the previous reaction is around 2600 K.

### 2.3.3. Influence of the new O–U modelling on the hyper-stoichiometric domain of the O–U–Zr ternary system

The new Gibbs energy parameters of the different phases of the O–U binary system are introduced in the NUCLEA database, the European thermodynamic database for corium applications [38]. From this database containing the modelling of the Gibbs energies of the phases with zirconium and the GEMINI2 [39] software, the isothermal sections of the O–U–Zr ternary system in the hyper-stoichiometric field $O–O_2U–O_2Zr$ at $T = 2673$ K and 3073 K for 1 atm. total pressure are calculated (Fig. 3). The hyper-stoichiometric liquid appears in this field around 2500 K, for 1 atm. total pressure, while it appears around 2400 K for 2 atm. total pressure. The impact of the total pressure on the temperature of appearance of liquid is due to the presence of the complex O–U gas phase ($G$) in equilibrium with the solid solution in the hyper-stoichiometric field $O–O_2U–O_2Zr$. The 100 K difference is directly linked to the one observed in the O–U binary system.

Experimental data were obtained by Punni et al. [40] on solidus and liquidus temperatures in the mixed oxides system $(U, Zr)O_{2+x}$ in the hyper-stoichiometric region. In the tests, the sample contained in a welded tungsten can ($\sim 2cm^3$) was heated by a controlled thermal ramp and the liquidus and solidus identified by arrests in the temperature versus time curves. Unfortunately, the authors identified after the tests, traces of reactions of sample with the W capsule, which makes uncertain the measurements of the solidus and liquidus. The experimental results are

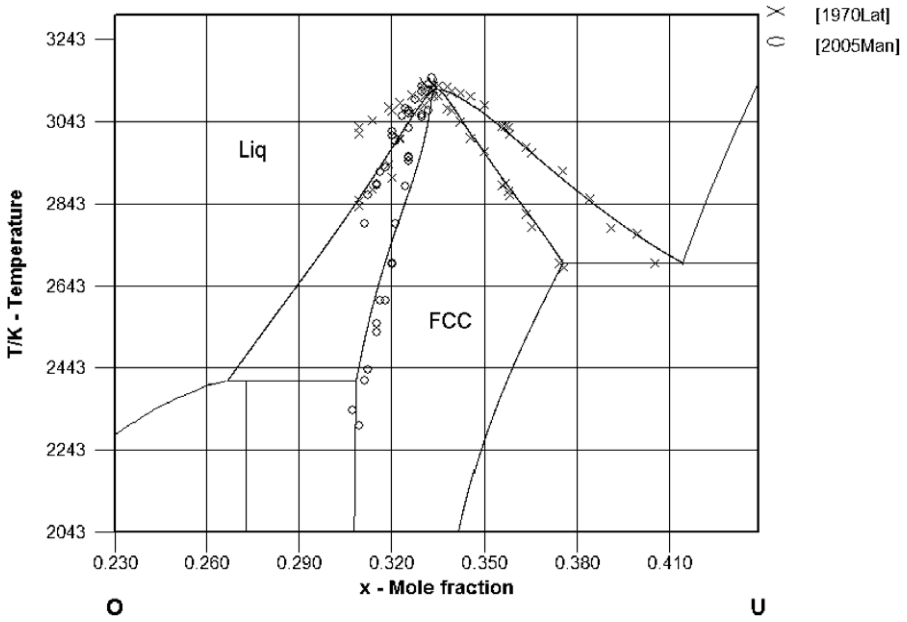


Fig. 2. Calculated phase diagram (without gas phase) of the O–U binary system with new optimized parameters in the hyper-stoichiometric field $UO_{2+x}$ with superimposed experimental data from [21,22].

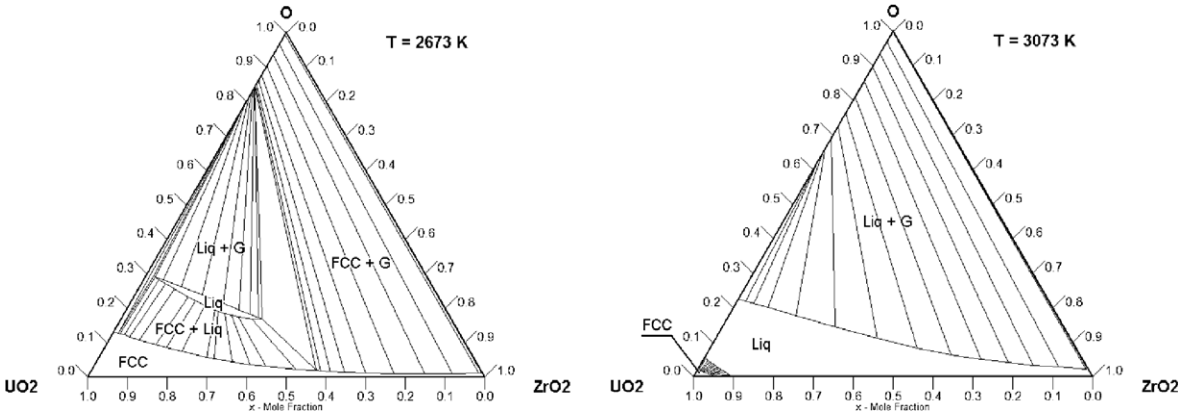


Fig. 3. Calculated O–$UO_2$–$ZrO_2$ region of the O–U–Zr system (fixed condition of $P_{tot} = 1$ atm.) (the gas phase is mentioned in the phase diagram only when the vapor pressure of the complex gaseous mixture of O–$O_2$–$O_3$–$O_3U$–$O_2U$–OU–U reaches the total pressure, i.e. 1 atm, otherwise it means that the vapor pressure is lower than one atmosphere).

Table 5
Liquidus and solidus temperatures determined by Punni [40] for the mixed oxides system $(U,Zr)O_{2+x}$ and comparison with the calculated values

| Composition | $T^L$ exp (K) | $T^L$ calc (K) | $T^S$ exp (K) | $T^S$ calc (K) |
|---|---|---|---|---|
| $(U_{0.65}Zr_{0.35})O_{2.000}$ | 2951 | 2950 | 2863 | 2890 |
| $(U_{0.65}Zr_{0.35})O_{2.052}$ | 2911 | 2880 | 2823 | 2660 |
| $(U_{0.65}Zr_{0.35})O_{2.098}$ | 2834 | 2820 | 2755 | 2470 |

summarized in Table 5 and compared to the calculated solidus and liquidus temperatures. Significant differences between the calculations (performed at a constant volume equal to 2 $cm^3$ considering the experimental conditions in the Punni's study; in these calculations, the Helmholtz energy instead the Gibbs energy is minimized) and the measurements are highlighted, in particular for the solidus temperatures. The calculated pressure in the can is about 10 atm. With this pressure, the calculated solidus temperatures are strongly reduced for hyper-stoichiometric fuel as it has been shown experimentally in [22]. At this point, we have to emphasize on the verticality of the liquidus and solidus shapes of the fluorite $(U,Zr)O_{2\pm x}$, as shown on Fig. 4 calculated with NUCLEA [38] and the GEMINI2 [39] software. A small variation of the deviation to stoichiometry during the experiment can have a considerable consequence on the liquidus and solidus temperatures. Considering the experimental uncertainties in the Punni's study, no definitive conclusion from the presented comparison can be drawn about the validation of the thermodynamic modeling of the hyper-stoichiometric field O–$O_2U$–$O_2Zr$ in the U–O–Zr ternary system.

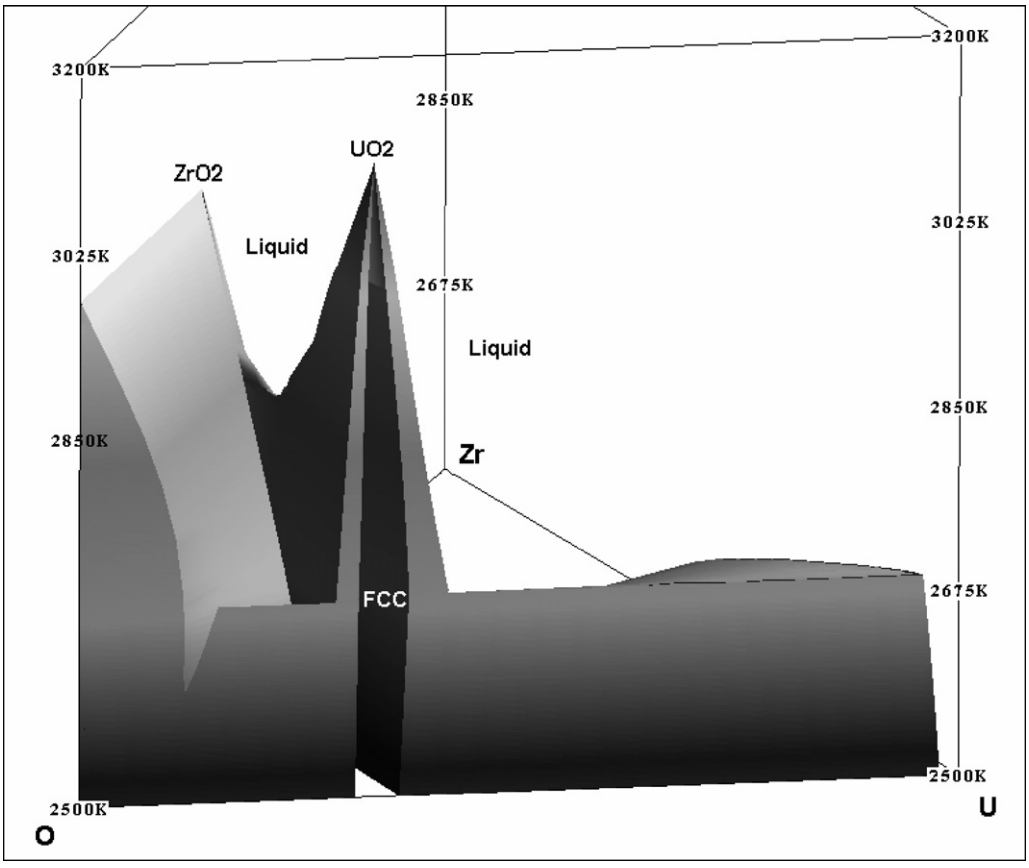


Fig. 4. Calculated 3D liquidus shape in the oxygen corner of O–U–Zr ($P = 1$ atm.).

## 3. Fuel rod liquefaction in oxidising conditions

### 3.1. Introduction

The VERCORS and PHEBUS FP tests evidenced liquefaction of fuel rod under oxidizing conditions at relatively low temperature, i.e. 200 to 300 K below the eutectic temperature of the $UO_2$–$ZrO_2$ phase diagram. In the following sections, are presented the experimental conditions in these tests, the identification of the fuel rod liquefaction process and the post-mortem examinations of the FPT1 PHEBUS test and the VERCORS tests related to the fuel rod liquefaction. These analyses allows to evaluate the extent of the fuel-cladding interaction and the impact of the fuel oxidation on the liquefaction process on the basis of the new modeling of the U–O–Zr phase diagram.

### 3.2. PHEBUS FP and VERCORS experiments

#### 3.2.1. Experimental conditions

The international PHEBUS Fission Product (FP) Programme has been conducted by the French 'Institut de Radioprotection et de Sûreté Nucléaire' (IRSN) within a framework of international cooperation. It investigates key phenomena occurring in light water reactor severe accidents by means of a series of in-pile experiments. The PHEBUS FP facility has been described in several papers [16,41]. The FPT0 bundle consisted of 20 fresh fuel rods, 1 m long, and an absorber rod (silver–indium–cadmium alloy), and the FPT1 bundle was made of 18 fuel rods irradiated at 23.4 GWd/tU and two instrumented fresh fuel rods maintained by two Zircaloy grids and an absorber rod. In both tests, the $UO_2$ fuel was pre-irradiated at low power for ~9 days in the PHEBUS facility in order to create an inventory of short-lived FPs. During these tests performed under total pressure of 2.2 atm., steam was injected, with a maximal flow rate of 3 g/s in FPT0 and 2.2 g/s in FPT1. In both tests, the first degradation event was the rupture of the fuel rod cladding [16,17]. The second was the degradation and rupture of the control rod between the Ni–Zr and Fe–Zr eutectic temperatures. Then, as temperatures increased, the fuel rod cladding oxidized, thus enhancing the temperature escalation: oxidation runaway began in both tests when the Zry cladding temperature reached ~1823 K. The increase in temperature during the subsequent oxidation period was smaller in FPT1 than in FPT0 (maximum temperature measured in FPT0 was about 2800 K and about 2500 K in FPT1), because the cladding had been more oxidised before the oxidation runaway. The atmosphere was in consequence significantly different at the oxidation peak in FPT0 (~10% $H_2O$/90% $H_2$ in moles) than in FPT1 (50% $H_2O$/

50% $H_2$). As temperatures increased, they became high enough to produce melting of non-oxidised Zr (melting point ~ 2000 K) or α-Zr(O) phase (melting point ~ 2200 K), and some material interactions as well (in particular fuel dissolution by liquid Zr), causing material relocation from the upper elevations. This material movement induced a temperature increase in lower zones where oxidation runaway can occur. After the oxidation period, the fuel was progressively heated up in both tests. The events occurring during this heat-up phase were attributed to successive relocations of liquefied materials (ceramic components including large quantities of uranium), and progressive formation of a molten pool in the lower part of the bundle. In both tests, the pool was approximately equimolar in $UO_2$ and $ZrO_2$. For FPT0, the melt composition was $(U_{0.51}Zr_{0.46}Fe_{0.03})O_{2\pm x}$ and for FPT1 it was $(U_{0.48}Zr_{0.48}Fe_{0.03}Cr_{0.01})O_{2+x}$. Post-test analysis showed a rather uniform melt composition in both cases with a primary (U, Zr, O)-based phase and some secondary phases (Fe, Cr, Ni)-based metallic or oxide precipitates.

Financed by IRSN in association with EdF (Electricité de France), the out-of-pile RT and HT VERCORS programme performed by the Commissariat à l'Energie Atomique (CEA) was devoted to the source term issue (i.e. the knowledge of the amount of radioactivity released from the core to the environment) of FPs released from PWR fuel samples (burn-up range between 38 and 70 GWd/tU) during conditions typical of severe accident up to loss of fuel geometry [15]. The samples usually consisted of three irradiated $UO_2$ pellets in their original Zircaloy cladding and were positioned in an induction furnace. Two half-pellets of depleted and un-irradiated uranium dioxide were placed at each end of the sample. The cladding was not fully sealed. Two tests (RT3 and RT4) were more specifically devoted to the behavior of debris bed (with $UO_2$ and $UO_2/ZrO_2$, respectively). Gamma detectors aimed at the top of the test section allowed to record the departure of FPs from fuel and to additionally detect the fuel degradation by measuring the loss of signal corresponding to non volatile FPs. In the test scenario, an oxidation plateau was performed at around 1770 K in order to fully oxidize the cladding before a temperature ramp up to very high temperatures and fuel melting or collapse. During the high temperature phase of the test, steam and hydrogen could be possibly injected with different flow rates through the internal channel containing the sample.

### 3.2.2. Fuel rod liquefaction

Due to the in-pile characteristics of the PHEBUS FP tests, detection of material movements cannot be performed in-situ. In addition during the heat-up phase of these tests, most of the thermocouples did not survive due to the high temperatures reached in the experimental section. For that reason, the identification of the fuel rod liquefaction and relocation is not straightforward. Nevertheless, the analysis of the thermal response of the PHEBUS FP bundle provides indications about these material movements which can be the results of partial or complete liquefaction of fuel. In FPT1, where the degradation was less pronounced than in FPT0, some thermocouples were still in live during the heat-up phase. Thermocouples inside the bundle not far from the mid-height plan (at 300 mm) in the peripheral zone of the test section indicated approximately 2300 K, i.e. approximately 2400–2500 K in the inner part of the test section, considering the thermal gradient along the azimuth. At this time, large increases of the heat-up rates in the response of the ultrasonic thermometer sensors located in the lower part of the bundle indicated that a major degradation event happened in the bundle. It suggests that successive relocations of liquefied materials (ceramic components including large quantities of uranium), accumulated onto the lower grid (240–280 mm) with the formation of a small molten pool likely occurred.

In the VERCORS tests [15], the detection of fuel melting (or collapse), could be more straightforwardly studied due to the experimental facility. In the different tests, it was detected for a temperature range of 2400–2600 K whatever the fuel burn-up. Whatever the respective flow rates of hydrogen and steam which varied from one test to another one, the temperature at which the fuel loses its cylindrical integrity was lower than both the melting temperature of fresh $UO_2$ (3120 K) and the $ZrO_2$–$UO_2$ eutectic temperature (2800 K).

### 3.2.3. Post-test examinations

In the PHEBUS FPT1 test, the fuel remnant compositions on both sides of the mid-height plan were measured using the electron micro-probe analysis (EMPA) technique [42]; they are reported in Table 6. At some elevations (607 mm), the fuel compositions generally reveal a significant amount of zirconium which exceeds the expected value of about 0.2 at.% due to fission and are explained by an interaction between fuel and cladding. Solid state interaction cannot be excluded but liquid cladding-fuel interaction is more probable. Indeed, micrographs of remaining irradiated pellets (Fig. 5) generally shows enlarged porosity not consistent with an assumed solid state interaction process. Around the mid-height plan (473 mm, Table 6), there was no trace of interaction between fuel and cladding. The fuel remnant composition can be considered as pure $UO_2$. The low level of zirconium inside is associated to the fission product.

Table 6
FPT1 test, fuel compositions measured at different elevations by EPMA (length of the fission column equal to 1 m)

| Fuel type | Level | Composition |
|---|---|---|
| Irradiated fuel | 473 mm | $(U_{0.99}Zr_{0.01})O_{2.23}$ |
| Irradiated fuel | 607 mm | $(U_{0.86}Zr_{0.12}Fe_{0.005}Cr_{0.001}Nd_{0.006}Pu_{0.004}Ce_{0.004})O_{2.42}$ |
| Fresh fuel | 607 mm | $(U_{0.95}Zr_{0.04}Fe_{0.001})O_{2.32}$ |

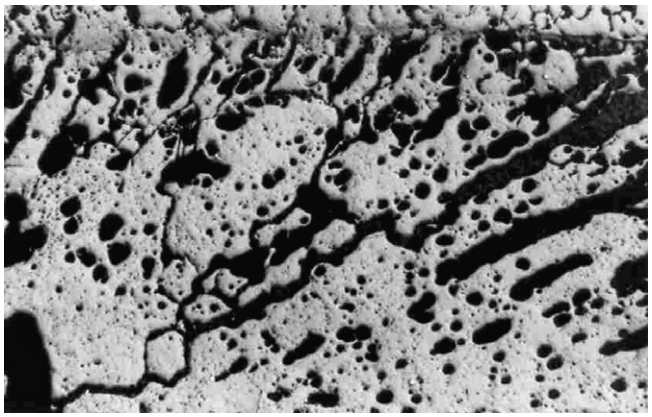

Fig. 5. FPT1 test, irradiated fuel morphology (607 mm) magnification 50×.

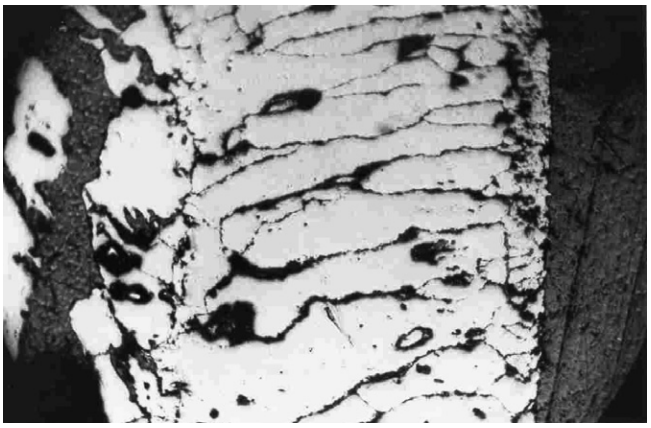

Fig. 7. FPT1 test, oxidized cladding morphology (607 mm) magnification 200×.

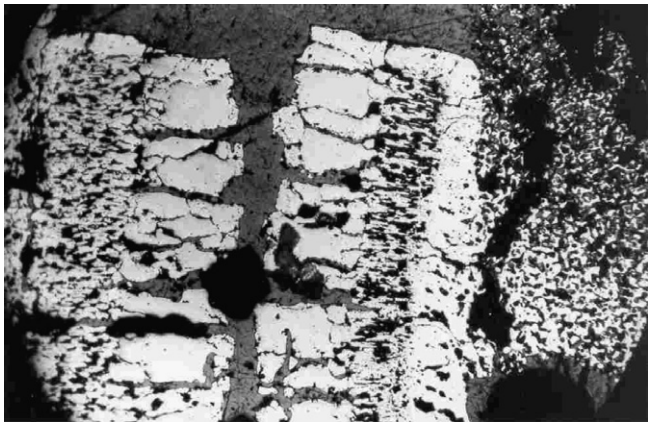

Fig. 6. FPT1 test, oxidized cladding morphology (473 mm) magnification 200×.

To understand these differences in fuel compositions, the morphologies of oxidized cladding must be examined. At 473 mm (Fig. 6), the Zry cladding exhibited a double-sided oxidation with numerous cracks in both longitudinal and traverse directions. This indicates that the cladding was already burst at the beginning of the oxidation runaway. The surface of oxidized cladding on both sides consisted of small oxide grains. They were formed during the slower prior oxidation whereas the larger columnar grains are due the intensive steam oxidation. This pre-oxidation prevented, at least in a first time, the fuel-cladding interaction. Another phenomenon which could have limited the interaction may be the flowering of the cladding by forming a gap between cladding and fuel. On the reverse, Zry cladding morphology at 607 mm (Fig. 7) did not reveal a double-sided oxidation but rather, all over its thickness, large grains typical of intensive oxidation. At the beginning of the oxidation phase, at this elevation, metallic or partially oxidized zirconium was available to interact with fuel.

From this analysis, it can be concluded that before fuel rod liquefaction, fuel composition was modified due to interaction with cladding but also due to oxidation by steam. Indeed, after significant clad rupture, the steam access to fuel was easier and it is quite sure that after clad oxidation, during the heat-up phase, the fuel hyper-stoichiometry was significant in the PHEBUS FP tests. A qualitative argument was given by the analyses of the metallic fission product precipitates (Mo–Ru–Tc–Rh–Pd) in the FPT1 corium showing that molybdenum usually was not present. It means that the oxygen potential was sufficiently high during the FPT1 test to oxidize Mo and consequently to oxidize $UO_2$, considering the respective positions of $U/UO_{2+x}$ and $Mo/MoO_2$ in the Ellingham diagram.

Table 6 gives the measured fuel stoichiometry at various elevations in FPT1 as obtained by EMPA technique [42]. One can observe a large dispersion in the measurements with some very high values. Calculations have been done to evaluate the probable fuel hyperstoichiometry during the PHEBUS FP tests. Thermodynamic equilibrium calculations have been firstly performed, using the detailed model for the U–O system (presented before) to determine the fuel stoichiometry at 2500 K in a pure steam atmosphere at a total pressure of 2.2 atm. They indicate that the oxygen/metal ratio would be about 2.11. According to a second calculation [43,44] taking into account both oxygen surface exchange and volume diffusion, i.e. using a kinetic rather a thermodynamic approach, the oxygen/metal ratio in fuel would be about 2.08 at 600 mm for a maximum temperature of 2600 K. For comparison, the deviations of fuel stoichiometry were about 2.14 for samples obtained from the molten core of the Three Mile Island Unit 2 (TMI-2) reactor [45] where the total pressure was higher than during the PHEBUS FP tests. These values lower than 2.25 (corresponding to $U_4O_9$), allow to conclude that at this temperature, oxides higher than $UO_{2+x}$ were not likely formed. On this basis, the large hyper-stoichiometries reported in Table 6 for 607 mm in the FPT1 test, must be cautiously considered. By contrast, the larger deviation to the stoichiometry in irradiated fuel in comparison with fresh fuel is compatible with observations of Imamura et al. [46] who measured higher oxidation rates for fuel of burn up of 27 GWd/tU (i.e. comparable with the burn-up of FPT1 fuel) than for fresh fuel. This analysis

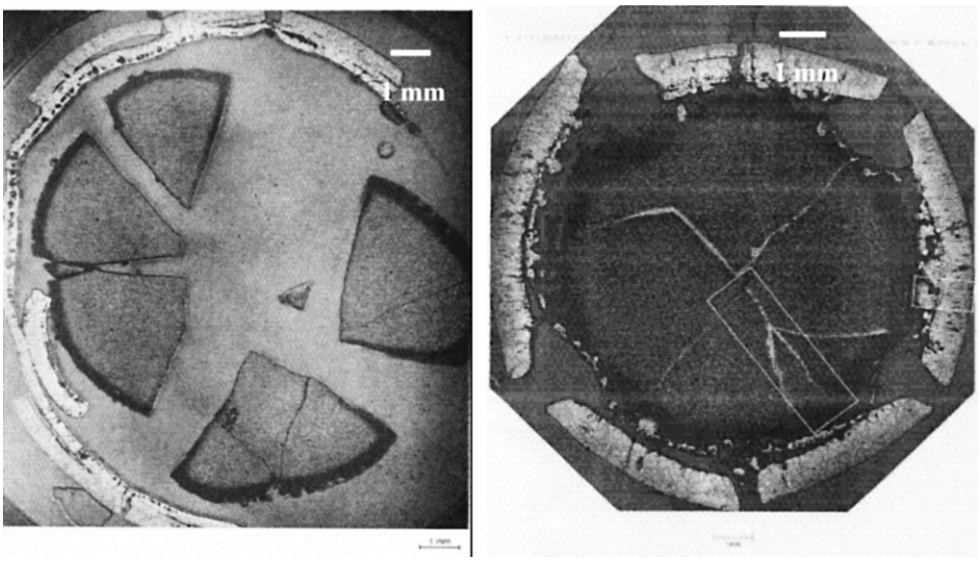


Fig. 8. Ceramographics of VERCORS 4 (left) and VERCORS 5 (right).

shows that fuel oxidation was highly probable during the PHEBUS FP tests.

After the VERCORS tests, ceramographic examinations of fuel were generally performed. The pictures given in [15] (here reproduced on Fig. 8) are instructive because they are representative of the behavior of a 38 Gwd/tU burn-up $UO_2$ fuel just before relocation. They gave, in particular, qualitative information about the extent of the interaction between fuel and cladding during the tests. In VERCORS 5 (Fig. 8, right), penetration of melts along the irradiated fuel cracks are clearly visible. They were attributed by Pontillon et al. [15] to fission products which are assumed to play an active role in the interaction between fuel and oxidized cladding, favoring the decrease of fuel 'collapse' temperatures. To our opinion, the fission products should not play a key role in the extent of these interactions, considering the relatively low amount of fission products in a 38 Gwd/tU burn-up fuel. Additionally, the localization of these melts along fuel cracks which are not known as preferential sites for fission products are not in favor of the assumption retained in [15]. These melts may have more likely their origin in an incomplete oxidation of the cladding before the high temperature phase of the VERCORS tests in spite of the oxidation plateau performed at 1770 K or in a solid state interaction between $UO_2$ and Zr during the oxidation plateau. Concerning the latter phenomenon, Dienst et al. [47] experimentally showed that the reduction of uranium dioxide by zirconium occurred in case of contact between both solids. At 1773 K, they showed that this interaction decisively depends on the contact between both solids, what could explain why these mixtures may be present in VERCORS 5 (Fig. 8, right) or absent in VERCORS 4 (Fig. 8, left), depending on the Zry/$UO_2$ contact in the tested samples.

These interactions could lead to an early fuel liquefaction at least in the VERCORS tests performed under pure $H_2$ atmosphere during the high temperature phase. Under steam or mixed $H_2O/H_2$ atmosphere these mixtures can be oxidized and then possibly solidified. At this stage of the post-mortem examinations in the VERCORS tests, it is not possible to go further in the evaluation of the impact of the interaction between Zry and $UO_2$ on the fuel collapse temperature. Nevertheless, one important fact in the VERCORS test series noted by Pontillon et al. [15], is the decrease of the fuel collapse temperature in oxidizing conditions in comparison with more reducing conditions. Additionally, in the RT4 test in which a $UO_2$-$ZrO_2$ debris bed was heated in oxidizing conditions, the cladding-fuel interaction could not be suspected below 2800 K and the fuel liquefaction temperature was measured around 2500–2600 K. Here, there are probably indications of the active role played by the fuel oxidation.

### 3.3. Discussion

The VERCORS and PHEBUS FP tests evidenced liquefaction (or collapse) of fuel rod under oxidizing conditions at relatively low temperature, i.e. 200–300 K below the eutectic temperature of the $UO_2$–$ZrO_2$ phase diagram. The *collapse* term is used in the VERCORS tests [15] to describe the loss of fuel geometry which may be the result of a partial or complete liquefaction. In fact, in both series of tests (VERCORS and PHEBUS), this term is appropriate considering the fact that the experimental observations are not indicative about the completeness of the fuel liquefaction. In this framework, solidus and liquidus temperatures are important bounds since they determine the temperature interval in which the loss of fuel geometry may happen.

In the VERCORS tests, the analysis of the respective impact of the fuel oxidation and the fuel-cladding interaction on the liquefaction process is not possible at this stage of the post-mortem examinations, in particular if one considers the absence of information on the fuel compositions.

On the contrary, in the PHEBUS FP tests, the impact of the interaction between Zry cladding and structural materials and fuel on these thresholds can be separately examined. The measured compositions reported in Table 6 show that iron (chromium) and zirconium were present in the remaining fuel pellets after the FPT1 test. The solidus temperature corresponding to an irradiated fuel of 23 GWd/tU with the following composition $UO_{2.00}$: 5–7 Zr at.% was measured using the same technique as in the Manara's paper by Ronchi et al. [29] at about $2950 \pm 20$ K, i.e. much higher than the observed fuel collapse temperature in FPT1. Uetsuka and Nagase [48] measured, by a thermal arrest method the melting temperature of simulated fuel debris samples having a similar chemical composition and porosity to TMI-2. The melting temperature was around $2840 \pm 20$ K. They concluded that the influence of minor constituents (mainly stainless steel oxides representing 7–8 wt.%) on the decrease in the melting temperature of $UO_2$–$ZrO_2$ compositions could be considered as negligible. According to the phase diagrams, FeO–$ZrO_2$ and FeO–$UO_2$, experimentally determined by Bechta et al. [32,49], stainless steel oxides could strongly reduce the solidus temperatures for $UO_2$–$ZrO_2$ compositions. Nevertheless, the amount of stainless steel and zirconium oxides measured inside the FPT1 fuel pellets (Table 6) seems too low to, *alone*, significantly decrease the solidus temperature.

On the basis of the new modeling of the U–O–Zr phase diagram (presented in Section 2), the impact of deviation to the stoichiometry (assumed to be between 2.08 and 2.11 considering the estimations in the previous section) on the solidus temperature might be stronger. The liquid phase for compositions representative of FPT1 irradiated fuel could be present at around 2600 K (solidus temperatures in Table 7). By contrast, the liquidus temperatures (Table 7) are very high, i.e. above 2900 K. It means that, at the fuel collapse temperatures as observed in the PHEBUS FP tests, the fuel would be only partially liquefied. At this stage, we can conclude that the possibility of fuel rod liquefaction at temperatures below 2800 K exists if fuel is oxidised.

To complete the analysis, the kinetics of the formation of liquid phase in the $(U,Zr)O_{2+x}$ system must be evaluated in conditions representative of fuel-cladding interaction. Some particular tests of the PHEBUS FP and VERCORS programmes can give insights into the liquefaction process in this system:

Table 7
Calculated liquidus and solidus temperatures for compositions representative of irradiated fuel remnants in the FPT1 PHEBUS test ($P = 2.2$ atm.)

| Composition | $T^L$ calc (K) | $T^S$ calc (K) |
|---|---|---|
| $(U_{0.88}Zr_{0.12})O_{2.000}$ | 3080 | 3020 |
| $(U_{0.88}Zr_{0.12})O_{2.08\text{-}2.11}$ | 2980–2960 | 2760–2660 |
| $(U_{0.87}Zr_{0.12}Fe_{0.01})O_{2.00}$ | 3060 | 2860 |
| $(U_{0.87}Zr_{0.12}Fe_{0.01})\ O_{2.08\text{-}2.11}$ | 2960–2920 | 2560–2460 |

– in the PHEBUS FPT4 test, a debris bed (composed of $UO_2$ and $ZrO_2$ particles representing fuel and oxidized cladding pieces) was long term annealed (during 1000 s approximately) at temperatures around 2900 K under a steam/hydrogen atmosphere. Post-mortem examinations [50] showed an inhomogeneous mixture with fully melted $(U,Zr)O_2$ phase and almost intact solid $ZrO_2$ and $UO_2$ with little diffusion of uranium and zirconium in them, respectively. The measured amount of zirconium (about 0.5 wt%) in pure $UO_2$ solid phase was likely too low to reduce the melting temperature of urania below the test temperature and it has led to not fully melted materials. Some of the compositions corresponding to the fully melted $(U,Zr)O_2$ phases found in FPT4 are similar to the FPT1 compositions in terms of U and Zr contents.
– in the VERCORS RT4 test, a debris bed with similar characteristics that PHEBUS FPT4 was annealed from 2300 K until the fuel collapse detection at 2500–2600 K. This period lasted about 1200 s.

On the other hand, the time between the onset of the fuel liquefaction at the mid-height plan of the FPT1 bundle and the completion of fuel accumulation on the lower grid of the bundle was evaluated at 1500 s. This duration is then of the same order of magnitude that the time necessary for the liquefaction processes observed in the VERCORS RT4 and PHEBUS FPT4. This analysis indicates that in FPT1, fuel rod liquefaction could take place within the heat-up phase of the test.

## 4. Conclusion

Measurements of liquidus and solidus of $UO_{2+x}$ have been recently obtained by Manara et al. [22]. These experimental data are in strong disagreement with the previous measurements of Latta and Fryxell [21]. In this paper, both sets of data have been critically analyzed and it has been shown, at this stage, that the technique used by Manara et al. (laser flash technique) allowed to overcome the main sources of difficulties encountered by Latta et Fryxell without rising other significant sources of uncertainties.

This analysis has suggested that the current modeling of the U–O phase diagram should be revised since it was, up to now based on the Latta et Fryxell's data. A new thermodynamic modeling of the U–O system in the hyper-stoichiometric region at high temperature has been then performed. The main quantitative change with regards to our previous work [23] is related to the calculation of the solidus temperatures for $UO_{2+x}$ which are strongly reduced.

The impact of the new Gibbs energy parameters of the different phases of the O–U binary system on the U–O–Zr phase diagram has been evaluated. The liquid phase appears in the O–$O_2U$–$O_2Zr$ hyper-stoichiometric field of the ternary system around 2500 K under atmospheric pressure. Further experiments in this field are necessary

to validate this evaluation which must be considered, today, only as an indication.

Nevertheless, these new results clearly rise the impact of the fuel oxidation on the fuel rod liquefaction in oxidizing conditions. Up to now, fuel-cladding interaction was considered to start at relatively high temperatures (2800 K) in these conditions. The VERCORS and PHEBUS FP tests evidenced liquefaction of fuel rod under oxidizing conditions at relatively low temperature, i.e. 200–300 K below the eutectic temperature of the $UO_2$–$ZrO_2$ phase diagram. In this paper, these experiments have been analysed and the role of the fuel oxidation on the fuel rod liquefaction highlighted. It has been shown that the fuel oxidation could, at least qualitatively, explain the reduction of the temperature of the start of the liquefaction process.

## References


[1] P. Hofmann, D. Kerwin-Peck, J. Nucl. Mater. 124 (1984) 80.
[2] P.J. Hayward, I.M. George, J. Nucl. Mater. 208 (1994) 35.
[3] P.J. Hayward, I.M. George, J. Nucl. Mater. 208 (1994) 43.
[4] P.J. Hayward, I.M. George, J. Nucl. Mater. 232 (1996) 1.
[5] P.J. Hayward, I.M. George, J. Nucl. Mater. 232 (1996) 13.
[6] D.R. Olander, J. Nucl. Mater. 224 (1995) 254.
[7] K.T. Kim, D.R. Olander, J. Nucl. Mater. 154 (1988) 85.
[8] K.T. Kim, D.R. Olander, J. Nucl. Mater. 154 (1988) 102.
[9] D.R. Olander, Nucl. Eng. Design 162 (1996) 257.
[10] D.R. Olander, W. Wang, J. Nucl. Mater. 247 (1988) 258.
[11] M.S. Veshchunov, P. Hofmann, A.V. Berdyshev, J. Nucl. Mater. 231 (1996) 1.
[12] A. Skokan, in: Proceedings of 5th International Meeting on Thermonuclear Reactor Safety, Karlsruhe, September 1984, p. 9.
[13] M.S. Veschunov, A.V. Berdyshev, J. Nucl. Mater. 252 (1998) 98.
[14] W.A. Lambertson, M.H. Mueller, J. Am. Ceram. Soc. 36 (11) (1953) 367.
[15] Y. Pontillon, P.P. Malgouyres, G. Ducros, G. Nicaise, R. Dubourg, M. Kissane, M. Baichi, J. Nucl. Mater. 344 (2005) 265.
[16] B. Clément, N. Hanniet-Girault, G. Repetto, D. Jacquemain, A.V. Jones, M.P. Kissane, P. von der Hardt, Nucl. Eng. Des. 225 (2003) 5.
[17] D. Jacquemain, S. Bourdon, M. Barrachin, A. Debremaecker, FPT1 Final Report, IP/00/479, 2000.
[18] F.C. Iglesias, B.J. Lewis, P.J. Reid, P. Elder, J. Nucl. Mater. 270 (1999) 21.
[19] J.L. Bates, J. Nucl. Mater. 36 (1970) 234.
[20] S. Yamanouchi, T. Tachibana, K. Tsukui, M. Oguma, J. Nucl. Sci. Technol. 25 (6) (1988) 528.
[21] R.E. Latta, R.E. Fryxell, J. Nucl. Mater. 35 (1970) 195.
[22] D. Manara, C. Ronchi, M. Sheindlin, M. Lewis, M. Brykin, J. Nucl. Mater. 342 (2005) 148.
[23] P.Y. Chevalier, E. Fischer, B. Cheynet, Calphad 28 (2004) 15.
[24] C. Gueneau, M. Baichi, D. Labroche, C. Chatillon, B. Sundman, J. Nucl. Mater. 304 (2002) 202.
[25] R.S. Roth, T. Negas, L.P. Cok, Phase Diagrams for Ceramists, vol. IV, American Ceramic Society, 1981 (Figures 5000–5590); Yu.V. Levinskii, Atom. Energy 37 (4) (1974) 339; Soviet Atom. Energy (Engl. Transl.) 37(4) (1974), 1075; Figure 5028.
[26] D. Manara, C. Ronchi, M. Sheindlin, R. Konings, J. Nucl. Mater. 362 (2007) 14.
[27] M. Baichi, C. Chatillon, G. Ducros, K. Froment, J. Nucl. Mater. 349 (2006) 17.
[28] M. Baichi, C. Chatillon, G. Ducros, K. Froment, J. Nucl. Mater. 349 (2006) 57.
[29] C. Ronchi, M. Sheindlin, Int. J. Thermophys. 23 (1) (2002) 293.
[30] D. Bottomley, M. Sheidlin, J. Somers, M. Murray, H. Thiele, W. Heinz, M. Steiberger, Melting point measurements of the suboxidised U–Zr–O system by laser heating for application to reactor accidents, in: Proceedings of the 11th International QUENCH Workshop, 25–27 October 2005, Forschungszentrum Karlsruhe, Germany.
[31] S.V. Bechta, V.B. Khabensky, V.S. Granovsky, E.V. Kroushinov, S.A. Vitol, V.V. Gusarov, V.I. Almiashev, L.P. Mezentseva, Yu. B. Petrov, D.B. Lopukh, M. Fischer, D. Bottomley, W. Tromm, M. Barrachin, E. Altstadt, P. Piluso, F. Fichot, S. Hellmann, F. Defoort, CORPHAD and METCOR ISTC Projects, in: Proceedings of ERMSAR, 14–16 November 2005, Aix en Provence, France.
[32] S.V. Bechta, E.V. Krushinov, V.I. Almjashev, S.A. Vitol, L.P. Mezentseva, Yu.B. Petrov, D.B. Lopukh, V.B. Khabensky, M. Barrachin, S. Hellmann, K. Froment, M. Fischer, W. Tromm, D. Bottomley, F. Defoort, V.V. Gusarov, J. Nucl. Mater. 348 (2006) 114.
[33] S. Yamanaka, M. Katsura, M. Miyake, S. Imoto, S. Kawasaki, J. Nucl. Mater. 130 (1985) 524.
[34] F. Dolezalek, Z. Phys. Chem. 64 (1908) 727.
[35] I. Prigogine, R. Defay (Eds.), Thermodynam. Chim., Dunod, Paris, 1950.
[36] B. Sundman, J. Agren, J. Phys. Chem. Solid 42 (1981) 297.
[37] P.Y. Chevalier, E. Fischer, B. Cheynet, J. Nucl. Mater. 303 (2002) 1.
[38] NUCLEA Database (Thermodata 2003–2008), (©Thermodata 2003–2008), <http://hal.archives-ouvertes.fr/hal-00165418>.
[39] B. Cheynet, P.Y. Chevalier, E. Fischer, Calphad 26 (2) (2002) 167.
[40] J.S. Punni, M.A. Mignanelli, AEA-T Internal Report AEAT/R/NS/0428, Enthalpy Project Report (5th Framework Programme of European Commission) SAM-ENTHALPY(01)-D004, 2001.
[41] M. Schwarz, G. Hache, P. von der Hardt, Nucl. Eng. Des. 187 (1999) 47.
[42] P.D. Bottomley, S. Brémier, D. Papaioannou, C.T. Walker, Mikrochim. Acta 139 (2002) 27.
[43] R. Dubourg, H. Faure-Geors, G. Nicaise, M. Barrachin, Nucl. Eng. Des. 235 (2005) 2183.
[44] B.V. Dobrov, V.V. Likhanskii, V.D. Ozrin, A.A. Solodov, M.P. Kissane, H. Manenc, J. Nucl. Mater. 255 (1998) 59.
[45] P.D. Bottomley, M. Coquerelle, Nucl. Technol. 89 (1989) 120.
[46] M. Imamura, K. Une, J. Nucl. Mater. 247 (1997) 131.
[47] W. Dienst, P. Hofmann, D. Kerwin-Peck, Nucl. Technol. 65 (1984) 109.
[48] H. Uetsuka, F. Nagase, Companion Sample Examination and Related Study at JAERI, in: Proceedings of an Open Forum, OECD/USNRC, 20–22 October 1993, Boston, United States.
[49] S.V. Bechta, E.V. Krushinov, V.I. Almjashev, S.A. Vitol, L.P. Mezentseva, Yu.B. Petrov, D.B. Lopukh, V.B. Khabensky, M. Barrachin, S. Hellmann, K. Froment, M. Fisher, W. Tromm, D. Bottomley, F. Defoort, V.V. Gusarov, J. Nucl. Mater. 362 (2007) 46.
[50] D. Gavillet, Paul Scherrer Institut (PSI) Internal Report, TM-43-05-20, 2006.